TITLE

mRNA stability factor HuR promotes immune evasion in pancreatic ductal adenocarcinoma

AUTHORS

Yifei Guo[1,2,3], Jennifer M. Finan[1,2,3], Alexandra Q. Bartlett[1,2,3], Shamilene Sivagnanam[2,3], Katie E. Blise[3], Nell Kirchberger[2,3], Konjit Betre[2,3], Kevin Hawthorne[3,4], Canping Chen[5,6], Aaron Grossberg[3,7], Zheng Xia[5,6], Lisa M. Coussens[2,3], Rosalie C. Sears[3,4], Jonathan R. Brody[1,2,3], Robert Eil[1,2,3]

[1]Department of Surgery, Oregon Health & Science University, Portland, OR, USA;

[2]Department of Cell, Developmental & Cancer Biology, Oregon Health & Science University, Portland, OR, USA;

[3]Brenden-Colson Center for Pancreatic Care, Knight Cancer Institute, Oregon Health & Science University, Portland, OR, USA;

[4]Department of Molecular and Medical Genetics, Oregon Health & Science University, Portland, OR, USA;

[5]Computational Biology Program, Oregon Health & Science University, Portland, OR, USA;

[6]Department of Biomedical Engineering, Oregon Health & Science University, Portland, OR, USA;

[7]Department of Radiation Medicine, Oregon Health and Science University, Portland, OR, USA.

ABSTRACT

The tumor microenvironment (TME) of pancreatic ductal adenocarcinoma (PDAC) is characterized by a limited infiltration of tumor-specific T cells and anti-tumor T cell activity. Extracellular factors in the PDAC TME have been widely reported to mediate immune suppression, but the contribution from tumor-intrinsic factors is not well understood. The RNA-binding protein, HuR (*ELAVL1*), is enriched in PDAC and negatively correlates with T cell infiltration. In an immunocompetent Kras-p53-Cre (KPC) orthotopic model of PDAC, we found that genetic disruption of HuR impaired tumor growth. Importantly, we found that HuR depletion in tumors enhanced both T cell number and activation states. Mechanistically, HuR mediated the stabilization of mTOR pathway transcripts, and inhibition of mTOR activity rescued the impaired function of local T cells. Phenotypically, we found that HuR induced T-cell suppression in PDAC, as HuR depletion sensitize PDAC tumors to immune checkpoint blockade, while isogenic, wildtype tumors are resistant. Our findings describe

28 a novel role of HuR in facilitating tumor immune suppression in the PDAC TME by inhibiting T cell infiltration and
29 function, and implicate HuR inhibition as a potential therapeutic combination with immunotherapy.
30
31 **SIGNIFICANCE**
32 This study identified a novel mechanism that HuR supports pancreatic tumor growth by restricting T cell infiltration,
33 promoting immune evasion. Our work supports targeting strategies against HuR in PDAC with the goal of enhancing PDAC
34 sensitivity to immune-based cancer therapies, such as checkpoint blockade and T cell transfer.
35
36 **INTRODUCTION**
37 Pancreatic ductal adenocarcinoma (PDAC) is one of the leading causes of cancer-related death worldwide with a 5-
38 year survival rate of 13%, underscoring the need to develop improved therapeutic strategies[1]. The complex tumor
39 microenvironment (TME) of PDAC is thought to hinder both chemo- and immunotherapy efficacy[2]. Despite the presence
40 of immunogenic neoantigens that are predicted to be recognized by endogenous T cells, PDAC has remained resistant
41 to immune checkpoint blockade (ICB)[3–5]. Some have proposed that the ability of cancer cells to downregulate antigen
42 presentation machinery is a major driver of evading T cell recognition in PDAC. However, only a small proportion (~1-2%)
43 of PDAC contain mutations within antigen presentation or processing machinery[6]. Even in patients with mismatch repair
44 deficient (MMR-D) driven PDAC, where neoantigen frequency is equivalent to other MMR-D cancers, ICB had
45 compromised rates of objective response in PDAC in comparison to other MMR-D cancers[7]. Thus, we and others have
46 concluded that unresolved tumor-intrinsic sources of T cell suppression exist in PDAC. Specifically, cytotoxic T cells in the
47 PDAC TME have characteristics of T cell dysfunction, such as an inadequate response to stimulation (hypo-responsiveness),
48 which is recognized as a major source of tumor immune escape[8–10]. Therefore, in PDAC, there remains a need to understand
49 and reverse the tumor specific mechanisms that drive resistance to cancer immunotherapies[11].
50 Investigators continue to appreciate that TME features, including cytokines and cell-cell interactions, can restrain
51 the antitumor functions of $CD4^+$ and $CD8^+$ T cells. In tumors, PDAC especially, a combination of rapid cellular proliferation
52 and pathologic extracellular architecture contribute to a microenvironment that is low in both glucose and oxygen[12,13].
53 Meanwhile, T cells depend on consumption of nutrients to effectively respond to TCR ligation with acquisition of effector
54 programs, production of cytokines, and target cell cytolysis. Thus, the tumor-imposed nutrient deficit results in a metabolic
55 competition with local immune cells, contributing to T cell hypo-responsiveness and resistance to immunotherapies[14]. As

56 others have increasingly appreciated the importance of nutrient availability and metabolism for effective T cell antitumor
57 function, interest continues to grow in therapies that could increase nutrient availability and consumption by tumor-specific
58 T cells[15].

59 In human PDAC and preclinical models, the RNA-binding protein, human antigen R (HuR, *ELAVL1*) is known to
60 be hyperactive, supporting multiple programmatic hallmarks of cancer[12,13,16,17]. Functionally, HuR recognizes and binds to
61 3' untranslated regions (UTRs) of transcripts, enhancing their stability and translation[18]. For instance, HuR reshapes the
62 metabolic profile of PDAC, in part, by stabilizing *IDH1* transcripts and reprogramming both glycolytic and
63 lipogenic metabolism[13,19,20]. Broadly, HuR activity is associated with Myc programs and glycolytic metabolism, enhancing
64 the activation of c-Myc programs and consumption of surrounding nutrients for growth in size and cell division[12,21,22].
65 Additionally, pancreas-specific HuR overexpression alone caused fibro-inflammation in the mouse pancreas and led to an
66 increase in precursor lesions of PDAC in cooperation with a $Kras^{G12D}$ mutation[23]. Our prior observations support a model
67 wherein tumor-intrinsic HuR can mediate cell-cell communication and alter the PDAC TME in immune compromised
68 models[13,24]. In the context of metabolic competition between tumor and immune cells, we hypothesized that tumor-intrinsic
69 HuR activity may drive a competitive metabolic advantage over neighboring T cells. Yet, due to a lack of murine PDAC
70 model that can capture the immune contexture with HuR depletion, the role of HuR in the PDAC-immune crosstalk has not
71 been examined[16,17,24].

72 Taken together, our prior works point to a hypothesis that HuR may have a substantial role in mediating immune
73 evasion in the PDAC TME. Moreover, we report here that HuR expression is negatively correlated with both T cell
74 infiltration and outcome in PDAC patients. Thus, we investigated whether depletion of HuR in PDAC would impact tumor
75 growth and anti-tumor immune activity in an immunocompetent model of PDAC. To this end, we developed an isogenic
76 $Kras^{G12D}$,$Trp53^{R172H}$,*Pdx1-Cre* (KPC) mutant-driven murine PDAC model, with and without HuR, to further elucidate the
77 impact of tumor-intrinsic HuR on the immune components of the PDAC TME[25]. We observed that tumors with disruption
78 in the *Elavl1* locus (HuR) had impaired tumor growth *in vivo*. To investigate the impact of the immune cells on tumor
79 growth, we analyzed the infiltrated immune population in tumors and found that HuR depletion in tumors led to increased
80 T cell infiltration and activation in the PDAC TME. Moreover, antibody-based depletion of $CD4^+$ and $CD8^+$ T cells restored
81 the *in vivo* growth of HuR-deficient KPC tumors, demonstrating that HuR is required for intact PDAC growth in the
82 immunocompetent setting. Introduction of a model antigen and assessment of tumor specific T cells identified that tumor-
83 intrinsic HuR deterred the infiltration of antigen-specific $CD8^+$ T cells and their acquisition of effector functionality.

84 Mechanistically, HuR mediated stabilization of mTOR pathway-related transcripts and enhanced PDAC nutrient
85 consumption to the detriment of local T-cell antitumor function. Consistent with such a model, inhibition of the mTOR
86 pathway in PDAC cells enhanced the cytokine production capacity of co-cultured $CD8^+$ T cells in an HuR-dependent
87 manner. Therapeutically, KPC tumor's resistance to ICB treatment was dependent on the presence of HuR, and HuR
88 depletion combined with ICB led to tumor regression. Herein, we provide a deeper understanding of a potent immune
89 suppression mechanism driven by the pro-oncogenic protein, HuR, in PDAC.
90

91 **METHODS**

92 *Single-cell data collection and analysis*

93 Single-cell RNA sequencing (scRNA-seq) data were sourced from the Deeply Integrated Single-Cell Omics
94 (DISCO) database[26]. A total of 115 PDAC samples, encompassing 557,304 cells, were utilized to investigate the relationship
95 between *ELAVL1* gene expression in malignant cells and lymphocyte infiltration. Malignant cells were identified using the
96 R package scATOMIC (v2.0.2)[27] with the parameter "known_cancer_type = PAAD cell" and default settings for other
97 parameters. Spearman's correlation analysis was conducted to assess the association between gene expression levels in
98 tumor cells and cell-type infiltration in each sample.
99

100 *HuR signature survival analysis*

101 Published HuR activity signature[17] was assessed for Kaplan-Meier analysis of overall survival in surgical-resected
102 PDAC patient dataset[28]. The dataset is available in dbGaP database under accession phs003597.v1.p1.
103

104 *Immunohistochemistry staining of tumors*

105 Mouse tissues were fixed in 4% PFA overnight at 4°C before embedding and 5 μm sectioning. As previously
106 described[24], paraffin-embedded histological sections were stained for HuR (Santa Cruz Biotechnology; sc-5261) overnight
107 at 4°C, followed by incubation with a biotinylated secondary antibody for 1 hour at room temperature. Color was developed
108 with DAB substrate (Vector Laboratories; SK-4100), and mount for imaging. Brightfield images were acquired by Zeiss
109 Axio slide scanner.
110

111 *Cell lines and virus*

112 The PDAC murine cell line, KPC8069 (Kras^{G12D}-Trp53^{R172H}-Pdx1Cre), was a gift from Dr. Michael Hollingsworth.
113 Cells were cultured in normal DMEM with 10% fetal bovine serum (Gibco) and 1% penicillin/streptomycin (Thermo
114 Scientific; 15070063). Cell lines were maintained at 37°C in 5% humidified CO_2. Cell lines were *Mycoplasma* tested
115 routinely using Mycoplasma Detection Kit (SouthernBiotech; 13100-01). Before any experiment, cells were passaged at
116 least twice after thawing.

117 For HuR re-expression, KPC8069 cells were transfected with ecotropic retrovirus either carrying codon-enhanced
118 *Elavl1* sequence or empty vector and supplemented with 1 μg/ml polybrene (Millipore Sigma; TR1003G). Cells containing
119 the target vectors were selected by hygromycin (Millipore Sigma; H3274) and validated for HuR expression with
120 immunoblotting. For ovalbumin (OVA) expression, KPC8069 cells were transfected with ecotropic retrovirus carrying the
121 full-length OVA sequence and supplemented with 1 μg/ml polybrene. Cells containing the target vectors were selected by
122 blasticidin (Alfa Aesar; J67216-XF) and validated for OVA expression with flow cytometry.

123 All ecotropic retroviruses are generated by packaging 20 μg of plasmid DNA synthesized by Genscript, Inc.
124 containing genes of interest in an MSCV derived γ-retrovirus backbone (derived from Addgene; 122727) along with 3 μg
125 pCL-Eco plasmid DNA (Addgene; 12371) with platinum-E ecotropic packaging cells (Cell Biolabs; RV-101) and
126 jetOPTIMUS transfection reagent (Avantor; 101000006).

127

128 *INDEL assessment*

129 For INDEL assessment, genomic DNA was harvested from cells at time of analysis using the DNeasy Blood and
130 Tissue DNA kit (Qiagen; 69504), and the region containing *Elavl1* short guide (sg) RNA target was PCR-amplified and
131 Sanger sequenced by Eurofins Genomics. For each sample, a 493-bp region was amplified for sequencing (forward primer:
132 5′-ACTGGGGCTGAAGAAAAGTAGT-3′, reverse: 5′-GAACTGAATCATCTCCCCGGT-3′). 100 to 200 ng of each
133 amplicon was sent for sequencing with 2 pmol of its respective sequencing primer (5′-
134 TAGTCTGAGGTTAAAGAACAAAACTTCATT-3′). The indel percentage of amplicons derived from HuR-KO cells was
135 deduced using the Synthego ICE tool (Synthego; ICE Analysis v3.0).

136

137 *Immunoblot analysis*

138 Cells were lysed using ice-cold RIPA buffer (Thermo Scientific; 89900) supplemented with protease inhibitors
139 (Thermo Scientific; 87786). Protein concentration was quantified using the Pierce BCA Protein Assay kit (Thermo

Scientific; 23225). Equal amounts of whole protein extracts were loaded and separated by electrophoresis on a 4% to 12% Bis-Tris gel (Invitrogen; NP0321BOX) and transferred to a PVDF membrane (Bio-Rad; 1704156). Blots were blocked in Intercept® (TBS) Blocking Buffer (LI-COR Biosciences; 927-70003) and then probed with antibodies against anti-HuR (1:1000, Santa Cruz Biotechnology; sc-5261) and anti-α-tubulin (1:5000, Invitrogen; A11126), followed by Thermo Fisher Scientific Alexa secondary antibodies. Immunofluorescence was measured using a digital imager (Invitrogen; iBright 1500).

RNA extraction and RT-qPCR

RNA was extracted using RNeasy Mini Kit (Qiagen; 74106). RNA concentrations and quality were assessed by NanoDrop spectrophotometer (Thermo Scientific). Complementary DNA (cDNA) was made from 500 ng RNA using High Capacity cDNA Reverse Transcriptase Kit (Thermo Scientific; 4368813). RT-qPCR was performed with SYBR green master mix (Thermo Scientific; 4385617) with HuR primers and cDNA. Amplification signal was captured by RT-qPCR machine (Thermo Scientific; QuantStudio 7 Flex). Relative quantifications were assessed using the Log_2–ΔΔCt method, using GAPDH for normalization.

Mouse experiments

Animal protocol # IP00003322 and #IP00003155 were approved by Institutional Animal Care Regulations and Use Committee of OHSU. These protocols are specifically applicable to the experiments reported in this manuscript. All mice were obtained from The Jackson Laboratory. C57BL/6 mice (Cat. 000664) of 8–9 weeks of age were used as recipient hosts for KPC tumor implantation. OT-I transgenic mice were used as OT-I T cell donors.

For T cell depletion studies, mice were intraperitoneally injected with αCD8 blocking antibody (200 μg, BioXcell; BE0061) and αCD4 blocking antibody (200 μg; BioXcell; BE0003-1) two days before tumor implantation. The treatment was maintained for the duration of the experiment by injecting every four days of αCD8 and αCD4 (100 μg each). For isotype controls, rat IgG2b (BioXcell; BE0090) at matching amount was used. This approach achieved >99% depletion of $CD8^+$ and $CD4^+$ T cells in spleens of T cell-depleted mice compared to control mice at endpoint.

For αPD-1 treatment, mice were intraperitoneally injected with αPD-1 blocking antibody (200 μg, BioXcell; BP0146) or isotype controls, rat IgG2a (BioXcell; BE0089) every 4 days. The first injections happened 5 days after tumor implantation, and each mouse received a total of 4 injections.

168 *Mouse PDAC tumor model*

169 For implantable tumor experiments, KPC tumor cells (1×10^6) were resuspended in 100 µl of 1:1 mixture of PBS
170 (Fisher Scientific; 14-190-250) and Matrigel (Fisher Scientific; 354234), injected subcutaneously into the flanks of mice,
171 and allowed to grow for 37 days. Tumor length and width were measured by caliper every four days.

172 For orthotopic tumor growth experiments, KPC tumor cells (4×10^4) were resuspended in 20 µl of 1:1 mixture of
173 PBS and Matrigel, orthotopically injected into the tail of mouse pancreas, and allowed to grow for 20 days. For orthotopic
174 tumor αPD-1 experiments, KPC tumor cells (9×10^4) were injected and allowed to grow for 15 days. Earlier endpoint
175 criteria included severe weight loss, or extreme weakness and inactivity. Tumor weight was measured by chemical scale
176 (Sartorius) at the endpoint.

177

178 *Flow cytometry and analysis*

179 Following euthanasia, tumors and spleens were promptly dissected, weighed, and stored in ice-cold PBS. Tumors
180 were subsequently minced with surgical scissors and dissociated with GentleMACS octo-dissociator and preset program
181 (m_impTumor_01, Miltenyi Biotec). The dissociated tumor was then filtered through a 40 µm filter. Spleens were mashed
182 and filtered through a 40 µm filter. All samples were ACK lysed for 60 seconds using ACK lysing buffer (Gibco; A1049201),
183 and then consolidated for staining.

184 Single-cell suspension of each sample was incubated with Live/Dead Fixable Aqua (Thermo Scientific; L34966)
185 and Fc block (BD; 553142) in PBS for 30 min at 4°C, followed by incubation with primary fluorochrome-labeled antibodies
186 at 4°C for 30 min in PBS with 0.5% BSA and 2 mM EDTA. For *ex vivo* cytokine production by T cell, samples were
187 incubated for 4 hours at 37°C with PMA (20 ng/mL, Sigma; P1585), ionomycin (1 µg/mL, Sigma; I0634), and GolgiStop
188 (BD; 554724). Intracellular staining was done using the Fixation/Permeabilization Kit (BD; 554722). Antibodies used in
189 flow analysis are listed in Supplementary Table 1. Flow cytometric analysis was performed on Cytek Aurora spectral
190 cytometer. Collected data were analyzed using FlowJo v10 (TreeStar).

191

192 *In vitro T cell activation and co-cultures*

193 Murine OT-I $CD8^+$ T cells were isolated from the spleens of OT-I transgenic mice (The Jackson Laboratory;
194 #003831) using the EasySep Mouse $CD8^+$ T cell Isolation Kit (Stemcell; 19853), which yielded an enrichment of 96%–
195 100% purity. Isolated $CD8^+$ T cells were stimulated *in vitro* with plate-bound anti-CD3 and anti-CD28 (5 µg/mL; BioXcell)

196 for 24 hours and expanded in RPMI-1640 (Gibco) completed with 10% FBS (Gibco), 1% nonessential amino acids (Gibco),
197 1% sodium pyruvate (Gibco), 1% penicillin/streptomycin (Gibco), 57 μmol/L 2-BME (Sigma), and 100 IU/mL of
198 recombinant human IL-2 (Peprotech).

199 For $CD8^+$ T cell co-culture with tumor cells, 50,000 $CD8^+$ T cells were incubated with 50,000 tumor cells in 96-
200 well round-bottom plates for 24 hours at 37°C with phorbol 12-myristate 13-acetate (PMA) (20 ng/mL, Sigma; P1585),
201 ionomycin (1 μg/mL, Sigma; I0634), and GolgiStop (BD; 554724). Intracellular staining was done using the
202 Fixation/Permeabilization Kit and antibodies used are listed in Supplementary Table 1. SIINFEKL tetramers were obtained
203 from the NIH tetramer core facility.

204

205 *RNA-sequencing*

206 RNA was isolated from frozen cells using RNeasy Mini Kit (Qiagen; 74106). RNA concentrations and quality were
207 assessed by NanoDrop spectrophotometer. Preparation of RNA library and transcriptome sequencing were conducted by
208 Novogene Co., Ltd using the HiSeq Illumina platform. Novogene analysis service aligned raw reads to GRCm38 genome
209 and performed DESeq2 differential expression analysis. Gene set enrichment analysis (GSEA) was done using GSEA v4.2.3
210 software with the MSigDB hallmark and curated gene sets[29,30].

211

212 *Ribonucleoprotein immunoprecipitation assay*

213 KPC cells were washed and harvested with cell scrapper in cold-PBS. Ribonucleoprotein immunoprecipitation
214 assay was done according to manufacturer's instructions (MilliporeSigma; 17-701) with modification to RNA purification.
215 Lysates were immunoprecipitated by using 10 μg of either anti-HuR antibody (Santa Cruz Biotechnology; sc-5261) or anti-
216 IgG control (MilliporeSigma; 12-371). For RNA purification from immunoprecipitation, the protocol was followed up to
217 the precipitation of RNA in ethanol, after which the entire mixture was transferred to an RNA column using the RNeasy
218 Micro Kit (Qiagen; 74004), and the manufacturer's instructions were followed thereafter. RNA quality was analyzed via
219 Bioanalyzer Pico chip by the Massively Parallel Sequencing Shared Resource Core at OHSU.

220 Preparation of RNA library and transcriptome sequencing were conducted by Novogene Co., Ltd using the HiSeq
221 Illumina platform. Novogene analysis service aligned raw reads to GRCm38 genome and performed HuR-enriched peak
222 annotation with MACS2 software[31]. KEGG (Kyoto Encyclopedia of Genes and Genomes) pathway enrichment analysis
223 was done on HuR-enriched peaks.

224

225 *Statistical analysis*

226 Data were analyzed using unpaired two-tailed Student's *t*-test and one-way ANOVA test. In all cases, two-tailed
227 tests with P values less than 0.05 were considered significant. Statistics were calculated using GraphPad Prism 10 software
228 (GraphPad Software Inc). Results were graphed as mean ± standard deviation for *in vitro* experiments and ± standard error
229 of mean for animal experiments. Experimental sample sizes were chosen using power calculations and preliminary
230 experiments. Samples that had undergone technical failure during processing were excluded from subsequent analysis.

231

232 *Data availability*

233 RNA-sequencing dataset is deposited at the GEO (Gene Expression Omnibus) database as GSE287307. RIP-
234 sequencing dataset is deposited as GSE287349.

235

236 **RESULTS**

237 *Tumor ELAVL1 (HuR) expression correlates with patient outcome and T cell infiltration in PDAC*

238 We previously demonstrated that the RNA-binding protein HuR is highly expressed and activated (i.e. translocated
239 to the cytoplasm) in PDAC compared to adjacent normal pancreas[24,32]. First, we applied a validated HuR activity signature
240 highlighting HuR-dependent transcripts[17] to a large RNA-sequencing dataset including surgical-resected PDAC patients[28],
241 and showed that a lower HuR target activity signature predicted significantly prolonged patient survival (**Fig. 1A**).
242 Separately, baseline immune infiltration has been demonstrated to be associated with overall prognosis and response to ICB
243 in a variety of cancers[33]. To further understand the relationship between HuR activity in PDAC and antitumor immune
244 activity, we assayed DISCO single-cell RNA sequencing datasets and found tumor-intrinsic HuR expression levels
245 negatively correlated with total $CD3^+$ lymphocyte infiltration, i.e. lower tumor-intrinsic *ELAVL1* mRNA levels were
246 associated with more abundant $CD3^+$ lymphocyte infiltration in patient samples (**Fig. 1B** and **C**). To determine the causative
247 relationship between tumor-intrinsic HuR and T cell infiltration, and antitumor function in PDAC, we used a syngenetic
248 implantable mouse model of PDAC (KPC)[25]. To first assess whether HuR activity is recapitulated in our KPC model as in
249 human PDAC, HuR protein expression and localization was visualized with IHC staining. In concordance with patient data,
250 the KPC tumors had higher expression of whole-cell HuR compared to the healthy mouse pancreas (**Fig. 1D** and **E**). These
251 findings support previous work that tumor-intrinsic HuR is a poor prognostic marker in PDAC and pro-oncogenic[17,34], and

252 in addition, negatively correlates with lymphocyte infiltration in PDAC. HuR is similarly elevated in the KPC model as in
253 human PDAC providing a strong rationale for the investigation of tumor-intrinsic HuR in this immunocompetent murine
254 PDAC model. To our knowledge, this is the first genetic assessment of the role of HuR in PDAC tumor *in vivo* in an immune
255 intact setting.
256
257 *Tumor-intrinsic HuR supports tumor growth in KPC model*
258 We first established KPC cells with CRISPR-Cas9 mediated *Elavl1* genetic deletion using electroporation of
259 scramble or *Elavl1* targeted sgRNAs complexed to purified recombinant Cas9 protein, as previously described[35]. We isolated
260 and expanded single cell clones from these KPC HuR knockout (KO) pooled cell lines and three clones with stable knockout
261 and proliferation performance were selected and used for subsequent analyses. We then validated and quantified CRISPR-
262 Cas9 mediated disruption of the *Elavl1* locus via insertion or deletion (INDEL) via Sanger sequencing for our isolated
263 clones (**Fig. 2A**). Accordingly, the clones had a significant reduction in HuR mRNA and lost HuR protein expression (**Fig.**
264 **2B** and **C**).
265 To determine the impact of HuR on PDAC progression *in vivo*, we subcutaneously implanted KPC cells subjected
266 to electroporation with scramble sgRNAs wildtype (WT) or sgRNAs targeting *Elavl1* (HuR-KO) into syngeneic C57BL/6
267 mice and tracked tumor growth over time. We found that the loss of tumor-intrinsic HuR significantly delayed growth over
268 time by area and by end point weight (**Fig. 2D** and **E**). However, Ki67 staining showed no difference in tumor cell
269 proliferation between these WT and HuR-KO tumors, suggesting that the decrease in tumor growth that resulted from the
270 loss of PDAC HuR was dependent on a tumor-host interaction (**Fig. 2F**). Importantly, re-expression of the *Elavl1* gene via
271 durable retroviral transduction in these HuR-KO cells rescued the tumor growth defect (**Fig. 2F** and **G**). Cumulatively, these
272 data causatively demonstrate, in genetic gain and loss of function, that HuR is required for PDAC progression *in vivo*.
273
274 *HuR-dependent growth of PDAC is immune mediated in vivo*
275 Our compiled analysis of TCGA cohorts identified a negative correlation between *ELAVL1* abundance and T cell
276 infiltration, suggesting that tumor-intrinsic HuR may act to constrain local immune activity and promote tumor progression.
277 To define the functional relationship between endogenous antitumor immunity and tumor-intrinsic HuR, we orthotopically
278 implanted KPC WT or HuR-KO into the pancreas of C57BL/6 hosts. We again observed a significant delay in growth in
279 the HuR-KO tumors in comparison to KPC WT tumors in this physiological-relevant stromal and immune

microenvironment (**Fig. 3A**). To provide a more granular understanding of the endogenous immune response, we performed enumerative and phenotypic assessment of intratumoral immune populations via flow cytometry. Our analysis revealed an increase in the abundance of $CD4^+$ T cells in KPC HuR-KO tumors as compared to WT tumors (**Fig. 3B**). We also observed an increase in $NK1.1^+$ T cells and $CD19^+$ B cells as a proportion of all $CD45^+$ leukocytes within HuR-KO tumors (Supplementary Fig. S1A). Phenotypic analysis of the tumor-infiltrating T cells demonstrated that both $CD4^+$ and $CD8^+$ T cells from HuR-KO tumors had a greater proportion expressing the transcription factor T-bet (*Tbx21*) (**Fig. 3C**). This is consistent with ongoing T cell effector function and polarization towards T helper Type 1 (T_H1) effector specification, the cell population responsible for antitumor activity[36]. Additionally, the percentage of $CD4^+$ $Foxp3^+$ regulatory T (T_{Reg}) cells trended lower in HuR-KO tumors compared to WT tumors, although not statistically significant (Supplementary Fig. S1B). Additionally, T cell surface phenotype markers CD25 and CD69 were more abundant on $CD4^+$ and $CD8^+$ T cells from HuR-KO tumors than WT tumors, suggestive of a more activated state in the HuR-KO tumors (**Fig. 3D**). Surface expression of antigen presentation major histocompatibility complex (MHC) class I, H2-kb, and immune checkpoint protein, PD-L1, on tumor cells was not significantly different between WT and HuR-KO tumors, suggesting HuR mediates immune suppression in this model independently of antigen presentation or the expression of co-inhibitory surface ligands (Supplementary Fig. S1C).

Lastly, to test the causal relationship between endogenous antitumor immunity and HuR-mediated tumor progression, we performed antibody-mediated depletion of $CD4^+$ and $CD8^+$ T cells from C57BL/6 hosts followed by orthotopic implantation of KPC tumors with or without HuR depletion. We found that depletion of $CD4^+$ and $CD8^+$ T cells restored the tumor growth of HuR-KO tumors, suggesting that the defect in tumor growth of HuR-KO PDAC is due to a comparative increase in endogenous T cell-mediated tumor control in the absence of tumor-intrinsic HuR (**Fig. 3A**). Together these data indicate that the tumor regression in the KPC HuR-KO tumors is mediated by presence of activated T cells, which are otherwise suppressed in WT conditions.

HuR restricts the effector functions of $CD4^+$ and $CD8^+$ T cells in PDAC

Drawing from our observation that tumor-intrinsic HuR suppressed the activation levels of PDAC-infiltrating T cells, we next asked whether HuR constrained the acquisition of effector functions of tumor-infiltrating T cells. To that end, we performed direct *ex vivo* reactivation of T cells infiltrating WT or HuR-KO PDAC tumors and captured and assessed their cytokine production via intracellular cytokine staining quantified by flow cytometry. By unsupervised clustering all

308 $CD4^+$ T cells based on their cytokine production, $CD4^+$ T cells derived from WT and HuR-KO tumors naturally separated
309 in two clusters demonstrating their distinct phenotypes (**Fig. 4A**). Consistent with increase in activation markers, $CD4^+$ T
310 cells derived from HuR-KO tumors exhibited increase in cytokine production and polyfunctionality (**Fig. 4A** and **B**).
311 Additionally, $CD8^+$ T cell derived from HuR-KO tumors displayed an increase in IFN-γ production compared to $CD8^+$ T
312 cells derived from WT tumors (Supplementary Fig. S2A).
313
314 *HuR restricts the infiltration of antigen-specific $CD4^+$ and $CD8^+$ T cells in PDAC*
315 To determine the impact of HuR loss in PDAC on the function and abundance of tumor-specific T cells, we
316 retrovirally transduced KPC cells with an ovalbumin (OVA)-expressing construct to make KPC cells express full-length
317 OVA for processing and presentation on MHC (**Fig. 4D**, left). When co-cultured KPC-OVA cells with *ex vivo* expanded and
318 activated T cell receptor (TCR) transgenic (OT-I) effector $CD8^+$ T cells specific for the ovalbumin SIINFEKL epitope
319 presented via H2kb MHC restriction. We found that KPC WT OVA cells exhibited suppression of OT-1 T cell cytokine
320 production (IFN-γ and TNF-α production) relative to KPC HuR-KO OVA cells (**Fig. 4C**), despite there being no difference
321 in MHC-I abundance or antigen presentation in KPC HuR-KO cells in response to interferon stimulation (**Fig. 4D**). This
322 co-culture model continues to support the notion that tumor-intrinsic HuR suppresses local T cell function in a manner
323 independent of antigen presentation or interferon response. To evaluate the endogenous T cell responses against the OVA
324 antigen in the presence or absence of tumor-intrinsic HuR, HuR WT or HuR-KO OVA cells were orthotopically implanted
325 into C57BL/6 mice. Notably, KPC HuR-KO OVA tumors were rejected in 80% of mice, with significantly smaller tumors
326 than KPC WT OVA tumors in those instances where a tumor was indeed evident (**Fig. 5D**). Given the absence of a pancreatic
327 tumor in most instances of HuR-KO KPC OVA, we evaluated the peritumoral tissues in both groups of tumor-bearing hosts.
328 We found statistically significant increases in the amount of $CD8^+$ T cells, and OVA tetramer$^+$ $CD8^+$ T cells in hosts bearing
329 HuR-KO OVA tumors than WT OVA tumors (**Fig. 4E)**. We observed much lower SIINFEKL tetramer staining in the spleen
330 of tumor bearing mice, and no difference in the amounts of OVA tetramer$^+$ $CD8^+$ T cells between spleens from WT tumor-
331 bearing hosts compared to HuR-KO tumor-bearing hosts (Supplementary Fig. S2B). Together these data indicate that tumor-
332 intrinsic HuR suppresses the number of functional populations (cytokine producing, and antigen-specific) of T cells in the
333 PDAC TME, thus promoting tumor immune evasion.
334
335 *HuR stabilizes anabolic transcripts and metabolic pathways*

336 To identify the mechanism underlying HuR-dependent immune suppression and tumor progression in our
337 immunocompetent model, we performed bulk-RNA sequencing on KPC WT and HuR-KO cells (Supplementary Fig. 3A).
338 GSEA analysis identified established signatures involved in MYC pathways and metabolic reprogramming, including
339 adipogenesis and cholesterol homeostasis, were higher in the KPC WT cells compared to the HuR-KO cells (Supplementary
340 Fig. S3A and B). Given that HuR is known to stabilize RNA by directly binding to the 3'UTR regions of transcripts, we
341 sought to identify those RNAs in the KPC WT cells using ribonucleoprotein immunoprecipitation (RIP) followed by high-
342 throughput RNA sequencing (**Fig. 5A**). We validated HuR-RIP pulldown with immunoblot analysis from the bead-bound
343 lysate and flow-through. Validating our protocol, motif analysis showed preferential binding to AU-rich sequences as
344 previously described for HuR (**Fig. 6C** and Supplementary Fig. 3C)[37]. Additionally, established HuR metabolism targets,
345 the *IDH1* 3' UTR[13], and the *Rictor* 3' UTR, demonstrated significantly peak enrichment in comparison to reference control
346 *GAPDH* loci (**Fig. 5B** and Supplementary Fig. 3D). KEGG pathway analysis of the 1847 bound mRNAs revealed
347 enrichment of transcripts involved in metabolism, including MAPK signaling, mTOR signaling, HIF1-α pathway and
348 proteoglycan pathways, consistent with a model wherein HuR drives PDAC nutrient consumption to the potential detriment
349 of adjacent cell populations (**Fig. 5D**).

350 To test our hypothesis that HuR increases mTOR activity and drives metabolic competition to suppress local T-cell
351 function, we pretreated KPC OVA cells with mTOR inhibitors (AZD8055 and Torin1) and IFN-γ, and then co-cultured the
352 pretreated KPC OVA cells with OVA-antigen specific OT-I cells (**Fig. 5E**). The pretreated KPC OVA cells had decreased
353 mTOR activity by the measurement of decreased levels of phosphorylated-ribosome subunit 6 (p-S6). Of note, we validated
354 that the inhibitors did not impair H2kb levels in these tumor cells (**Fig. 5F**). Confirming our hypothesis, we observed that
355 OT-I T cells co-cultured with mTOR-inhibited KPC WT OVA cells had increased cytokine production (IFN-γ and TNF) in
356 comparison to T cells co-cultured with vehicle-treated KPC WT OVA cells (**Fig. 5G** and **H**). In comparison, T cells co-
357 cultured with KPC HuR-KO OVA cells demonstrated higher cytokine production *de novo,* independent of additional mTOR
358 inhibition – suggesting overlap between the two pathways (**Fig. 5G** and **H**). This data further supports our hypothesis that
359 HuR-KO tumor cells have lower mTOR activity at baseline and as a result, less nutrient competition with T cells, thus
360 mTOR inhibition in HuR-KO tumor cells could not increase T cell function further. In addition, because of the different
361 inhibition capacity of different inhibitors, T cells co-cultured with tumor cells treated with mTOR1 and mTOR2 inhibitor,
362 Torin1, displayed increase in both IFN-γ and TNF production, while mTOR1 inhibitor, rapamycin, only displayed increase
363 in TNF production (**Fig. 5G** and **H**). Taken together, these data indicate mechanistically tumor-intrinsic HuR directly binds

364 to and stabilizes transcripts involved in mTOR pathways, and the HuR-mediated increase of mTOR activity in tumor
365 metabolic competes with local T cells and ultimately suppress T cell function.
366
367 *PDAC resistance to Immune checkpoint blockade is dependent on HuR*
368 As previous discussed, ICB showed limited response in PDAC patients with deficiency in DNA mismatch repair
369 machinery[7], which suggested that the PDAC TME is inherently immune suppressive. Drawing from the observation that
370 PDAC HuR is responsible for constraining the infiltration and function of tumor specific T cells, we next asked whether
371 PDAC therapeutic resistance to ICB treatment was dependent on HuR function. Following a published treatment regimen[3],
372 we treated KPC WT and HuR-KO tumors-bearing mice with αPD-1 or control αIgG (**Fig. 6A**). Consistent with prior reports,
373 αPD-1 treatment alone in KPC WT tumors did not lead to tumor regression. However, αPD-1 treatment in KPC HuR-KO
374 tumors induced significant and almost total tumor regression (**Fig. 6A**). The αPD-1 treatment did not induce significant loss
375 of body weight in mice, indicating the treatment was well-tolerated in both groups (**Fig. 6B**). Consistent with previous
376 observations (**Fig. 3A**), HuR depletion led to increased $CD4^+$ T cell infiltration in tumors. While αPD-1 treatment in HuR-
377 KO tumors did not further boost the $CD4^+$ T cell infiltration compared to the IgG treatment, interestingly, αPD-1 treatment
378 in HuR-KO tumors induced higher infiltration of $CD8^+$ T cells with no effect observed in the WT tumors (**Fig. 6C**). Together,
379 these data indicate that $CD8^+$ T cells are the main responder to αPD-1 treatment in HuR-KO tumors, and support our
380 hypothesis that HuR depletion in PDAC tumors provides a greater proportion of T cells in the TME, which increased the
381 capacity for enhanced antitumor effector activity.
382
383 **DISCUSSION**
384 The immune landscape of PDAC TME is highly immunosuppressive and is a major barrier to effective
385 immunotherapy response[2,8]. Hence, understanding the underlying molecular mechanisms is key to advancing
386 immunotherapy strategies. From multi-omics analysis on large patient databases, the RNA-binding protein, HuR, negatively
387 correlates with both patient survival and total lymphocytes infiltration in PDAC. Herein, we found that HuR expressed by
388 PDAC promotes tumor growth in the immunocompetent PDAC model. Within PDAC cells, HuR directly binds to and
389 stabilizes anabolic transcripts, ultimately limiting the abundance and function of $CD4^+$ and $CD8^+$ T cells. As the primary
390 mediators of antitumor immunity, the T cells in the HuR-proficient PDAC TME had limited effector functions in cytokine

391 production and antigen-specific response. This mechanism could be exploited with therapeutic potential, as depletion of
392 HuR sensitizes PDAC tumor to ICB treatment with increase efficacy.

393 In previous studies, loss of HuR in human PDAC xenografts in immunocompromised hosts had no impact on tumor
394 growth[24], which complements our findings that HuR has an immune-mediated tumor suppressive role. In addition, previous
395 work targeting overexpressing HuR in the mouse pancreas lead to chronic inflammation in the TME and promoted tumor
396 development, indicating HuR contributes to an unbalanced inflamed environment[23]. Herein, this is the first report of PDAC
397 tumor-intrinsic HuR having a potent extrinsic effect on the immune cells in the TME. This new discovery of HuR function
398 fits with its known role in supporting tumor initial and tumor progression, and future study should investigate how HuR-
399 mediated immune suppression promotes PDAC initiation from pancreatitis. Similarly, another key transcriptional regulator
400 in PDAC, Myc, has been shown to control immune evasion in PDAC[11]. Therefore, studying pro-oncogenic molecules like
401 HuR and Myc in immune-competent models may provide a much-needed understanding of the post-transcriptional and
402 transcriptional tumor-intrinsic networks involved in immune suppression in the PDAC TME.

403 Interestingly, we did not observe a high correlation between gain/loss of RNA transcripts by RNA-sequencing and
404 alignment abundance on RNA-immunoprecipitation. Overlapping these HuR-bound targets with those whose expression
405 was reduced upon HuR-KO in the same cell lines identified 141 RNAs that are dependent on HuR binding to maintain
406 transcript levels (data not shown). While the low percentage of overlap was surprising, published works have observed
407 similar non-linear relationships between RNA-binding proteins and their targets[37,38]. These results further illustrate the
408 complicated regulation mechanisms of RNA-binding proteins with its binding targets in general. A more granular
409 understanding of the relationship between HuR 3' UTR binding and the impact on protein abundance will inform our ability
410 to leverage HuR function for translational purposes.

411 Transcriptomic analyses in our KPC model confirmed multiple dysregulated pathways, which have been previously
412 illustrated to be regulated by HuR[16,17]. Specifically, HuR directly upregulates multiple pathways in tumor remodeled
413 metabolism[13]. Metabolic reprogramming in the tumor through the Warburg effect, characterized by aerobic glycolysis, not
414 only enhances tumor proliferation but also depletes the limited resources within the TME[14,39]. Recent metabolite profiling
415 of the PDAC interstitial fluid showed altered nutrient availability and nutrient deprivation in the PDAC TME[40], suggesting
416 metabolic competition could be one of the mechanisms that tumor cells use to suppress immune cell function. Particularly,
417 reports have shown that activated T cells need to reprogram their glucose and lipid metabolism to support their effector
418 functions[41,42], and Tregs are more adapted to glucose deprivation with an increase in fatty-acid oxidation[43]. These required

419 nutrients are in concordance with the HuR-mediated dysregulated metabolic pathways, suggesting HuR mediates immune
420 suppression via metabolic competition in the PDAC TME. In lieu of this, previous finding that PDAC WT and HuR-KO
421 tumors grow similarly in immunocompromised model further supports the notion that HuR-mediated anabolic pathways do
422 not support tumor growth by proliferation[24], instead by inducing immune suppression. In total, our results warrant further
423 exploration to define the mechanistic connection between HuR-mediated PDAC metabolism and T cell function and
424 differentiation in the TME.

425 In the PDAC immune landscape, our findings once again demonstrate the potential of $CD8^+$ T cells to be harnessed
426 for PDAC tumor control, while also highlight that $CD4^+$ T cells can play a crucial role in addition to well-described $CD8^+$
427 T cells. Similar observations of $CD4^+$ T cell having anti-PDAC response were found in the setting of αCD40 stimulation[44].
428 These findings support the potential of targeting $CD4^+$ T cells to augment anti-tumor responses. Other than T cells, tumor-
429 intrinsic HuR has broader impact on the immune landscape of the PDAC TME by increasing B cell infiltration and
430 decreasing dendritic cell populations (data not shown). One recent study identified an immunosuppressive subset of
431 dendritic cells in the PDAC TME, which could account for the phenotype we observed[45]. Still, the implications of these
432 findings highlight the need for further investigation into the role of non-T cell immune cells.

433 Broadly, these findings advance the paradigm that tumor-intrinsic mechanisms limit T cell infiltration and the
434 efficacy of anti-tumor immunity within the TME. Specifically, we highlight a novel role of tumor-intrinsic HuR as a
435 modulator of PDAC immune evasion. Currently, targeting strategies against HuR are under development (e.g., siHuR
436 nanotherapies and small molecule inhibitors)[46], and could potentially break PDAC resistance to immune-based anti-cancer
437 therapies (i.e., checkpoint blockade and T cell transfer) as demonstrated here in our pre-clinical KPC model. Because HuR
438 also has cell-intrinsic functions in intratumoral immune populations, further work will be required to understand the
439 combined impact of HuR inhibition on tumor control.

440

441 **FIGURE LEGENDS**

442 **<u>Figure 1.</u> Tumor ELAVL1 (HuR) expression correlates with patient outcome and T cell infiltration in PDAC**

443 **(A)** Kaplan-Meier plots demonstrating proportional overall survival in PDAC patients (n = 199) distinguished by low versus
444 high HuR Activity Signature.

445 **(B)** Scatter plot showing the Spearman's correlation between ELAVL1 expression in tumor cells and lymphocyte infiltration,
446 including CD8+ T cells, CD4+ T cells, and NK cells (n = 115 patients) and **(C)** violin plot demonstrating the difference in
447 lymphocyte infiltration in HuR- low and HuR-high tumors from the same samples.
448 **(D)** Representative images from patient tumor microarrays and KPC tumors stained for HuR expression and **(E)**
449 quantification of HuR protein staining intensity of normal pancreas, KPC GEMM (n=3) and xenograft tumors (n = 8).
450 Error bars represent standard error of the mean. ns, not significant; **P < 0.01; ***P < 0.005; ****P < 0.001, unpaired 2-
451 tailed Student's t tests **(C,E)**.
452
453 **Figure 2**. **Tumor-intrinsic HuR supports tumor growth in KPC model**
454 (**A**) INDEL quantification of single-cell clones isolated from CRISPR-Cas9 mediated disruption of the *Elavl1* locus in
455 KPC8069 tumor cells and (**B**) quantification of mRNA abundance by RT-qPCR and (**C**) protein abundance by immunoblot
456 of the same clones.
457 (**D**) Rates of subcutaneous KPC tumor growth represented over time following implant of KPC WT and HuR-KO tumor
458 cells (n = 5) . (**E**) Summary quantification and pictures of the final tumor weight and size on day 34.
459 (**F**) Quantification of the percentages of Ki67^{+} cells in total non-immune cells in subcutaneous KPC tumors by flow
460 cytometry (n = 5) .
461 (**G**) Histogram and quantification of flow cytometry analysis of HuR expression in KPC WT and HuR-KO tumor cells
462 retrovirally transduced with empty vector or HuR-overexpression vector prior to subcutaneous implantation to C57BL/6
463 hosts (n = 10). (**H**) Summary quantification of the final tumor weight on day 30.
464 Error bars represent stand deviation (**B,F**) and standard error of the mean (**D,E,F,G,H**). *P < 0.05; **P < 0.01; ****P <
465 0.001, one-way ANOVA test (**B,G,H**), unpaired 2-tailed Student's t tests (**D,E,F**).
466
467 **Figure 3**. **HuR-dependent growth of PDAC is immune mediated *in vivo***
468 (**A**) Representative flow cytometry illustrating enumerating T cells in host spleens treated with IgG or αCD4/8 before and
469 during orthotopic tumor implantation and summary analysis of final KPC WT and HuR-KO tumor weight in host with or
470 without T cell depletion (n = 6) .
471 (**B**) Summary analysis enumerating tumor infiltrating lymphocytes (TIL) in orthotopic KPC WT and HuR-KO tumors (n =
472 5).

473 (**C**) Summary data depicting CD4 and CD8 T-cell Tbet$^+$ percentages and (**D**) representative flow cytometry plot and
474 summary data depicting CD25 and CD69 phenotypic states on CD4 and CD8 T cells as in (**B**).
475 Error bars represent standard error of the mean. *P < 0.05; **P < 0.01; ***P < 0.005; ****P < 0.001, one-way ANOVA test
476 (**A**), unpaired 2-tailed Student's t tests (**B,C,D**),
477
478 **<u>Figure 4</u>. HuR restricts the function and infiltration CD4 and CD8 T cells in PDAC**
479 (**A**) Concatenated single-cell overlay and colorimetric density tSNE based depiction of the indicated proteins by flow
480 cytometry, and (**B**) representative and summary quantification of cytokines following *ex vivo* stimulation of isolated CD4$^+$
481 T cells from KPC WT and HuR-KO tumors (n = 5).
482 (**C**) Representative flow cytometry plot and summary data depicting cytokine productions of OT-I CD8$^+$ T cells co-cultured
483 with KPC WT OVA or KPC HuR-KO OVA tumor cells (n = 3).
484 (**D**) Representative flow cytometry plot depicting HuR expression and Kb-SIIN staining of KPC WT OVA or KPC HuR-
485 KO OVA tumor cells prior to orthotopic implantation, and summary data of tumor rejection rate and final tumor weight at
486 day 20. (**E**) Representative flow cytometry plot and summary data enumerating spleen and pancreas infiltrating CD8$^+$ T
487 cells and SIIN$^+$ CD8$^+$ T cells from KPC WT OVA and KPC HuR-KO OVA tumor-bearing mice (n = 5).
488 Error bars represent stand deviation (**C**) and standard error of the mean (**B,D,E**). *P < 0.05; **P < 0.01; ***P < 0.005; ****P
489 < 0.001, unpaired 2-tailed Student's t tests.
490
491 **<u>Figure 5</u>. HuR stabilizes anabolic transcripts and metabolic pathways**
492 (**A**) Schematic depicting RIP-seq process to identify HuR-bound transcript (n = 3). (**B**) RIP-seq reads genome alignment
493 plot to *IDH1 and Rictor* loci (3'UTR region highlighted with red box). (**C**) Representative immunoblot validation of HuR
494 pulldown in KPC cells in comparison to IgG control. (**D**) Summary depiction of enrichment scores (RichFactor) of KEGG
495 pathways with transcripts comparatively enriched in HuR-IP samples.
496 (**E**) Schematic depicting the pre-treatment of tumor cells with mTOR inhibitors (Rapamycin and Torin1) and IFN-γ before
497 co-culture with OT-I T cells. (**F**) Representative flow cytometry plot depicting *p*-S6 and H2-Kb staining of KPC WT OVA
498 cells after mTOR inhibitors and IFN-γ treatments. (**G**, **H**) Summary data depicting cytokine productions of OT-I CD8$^+$ T
499 cells co-cultured with pre-treated KPC WT OVA or KPC HuR-KO OVA tumor cells (n = 3).
500 Error bars represent stand deviation (**G**, **H**). *P < 0.05; ***P < 0.005; ****P < 0.001, one-way ANOVA test.

501

502 **<u>Figure 6</u>. PDAC resistance to Immune checkpoint blockade is dependent on HuR**

503 (**A**) Schematic for αPD-1 treatment on KPC tumor bearing mice, and summary data on final tumor weight at day15. (**B**)

504 Body weight of mice in (**A**) by group tracked over time (n = 4).

505 (**C**) Summary analysis enumerating tumor infiltrating lymphocytes (TIL) of KPC WT and HuR-KO tumors in mice received

506 IgG or αPD-1 treatment in (**A**).

507 Error bars represent standard error of the mean. *P < 0.05; **P < 0.01, unpaired 2-tailed Student's t tests (**A**), one-way

508 ANOVA test (**C**).

509

510 **<u>Supplement Figure 1</u>. Tumor-intrinsic HuR mediates immune composition in the PDAC TME.**

511 (**A**) Summary analysis enumerating tumor infiltrating NK cells, B cells, dendritic cells, macrophages, and (**B**) $Foxp3^+$ CD4

512 T-cell percentages. (**C**) Summary data depicting H2-kb and PD-L1 expression on non-immune cells in orthotopic KPC WT

513 and HuR-KO tumors (n = 5).

514 Error bars represent standard error of the mean. *P < 0.05; ***P < 0.005, unpaired 2-tailed Student's t tests.

515

516 **<u>Supplement Figure 2</u>. HuR restricts the function and infiltration CD4 and CD8 T cells in PDAC**

517 (**A**) Summary quantification of IFN-γ production following *ex vivo* stimulation of isolated CD8+ T cells from KPC WT and

518 HuR-KO tumors (n = 5).

519 (**B**) Summary data enumerating spleen infiltrating CD8 T cells and SIIN $tetramer^+$ CD8 T cells from KPC WT OVA and

520 KPC HuR-KO OVA tumor-bearing mice (n = 5).

521 Error bars represent standard error of the mean. **P < 0.01, unpaired 2-tailed Student's t tests.

522

523 **<u>Supplement Figure 3</u>. HuR stabilizes anabolic transcripts and metabolic pathways**

524 (**A**) Schematic and volcano plot depicting whole-transcriptomic changes between KPC WT and KPC HuR-KO tumor cells

525 (n = 3). (**B**) Summary depiction of normalized enrichment scores (NES) of gene-sets with transcripts comparatively enriched

526 or lost between indicated groups.

527 (**C**)Top 2 motif enrichment sequences from HuR-IP targets. (**D**) RIP-seq reads genome alignment plot to *GAPDH* locus

528 (3'UTR region highlighted with red box).

529 FDR q-value < 0.05, weighted Kolmogorov–Smirnov statistic test (**B**).

530

531 **REFERENCES**

532 1. Siegel RL, Miller KD, Wagle NS, Jemal A. Cancer statistics, 2023. *CA Cancer J Clin*. 2023;73(1):17-48.
533 doi:10.3322/caac.21763

534 2. Polani F, Grierson PM, Lim KH. Stroma-targeting strategies in pancreatic cancer: Past lessons, challenges and
535 prospects. *World J Gastroenterol*. 2021;27(18):2105-2121. doi:10.3748/wjg.v27.i18.2105

536 3. Evans RA, Diamond MS, Rech AJ, et al. Lack of immunoediting in murine pancreatic cancer reversed with neoantigen.
537 *JCI Insight*. 2016;1(14). doi:10.1172/jci.insight.88328

538 4. Freed-Pastor WA, Lambert LJ, Ely ZA, et al. The CD155/TIGIT axis promotes and maintains immune evasion in
539 neoantigen-expressing pancreatic cancer. *Cancer Cell*. 2021;39(10):1342-1360.e14. doi:10.1016/j.ccell.2021.07.007

540 5. Bailey P, Chang DK, Forget MA, et al. Exploiting the neoantigen landscape for immunotherapy of pancreatic ductal
541 adenocarcinoma. *Sci Rep*. 2016;6(1):35848. doi:10.1038/srep35848

542 6. Concha-Benavente F, Srivastava R, Ferrone S, Ferris RL. Immunological and clinical significance of HLA class I
543 antigen processing machinery component defects in malignant cells. *Oral Oncol*. 2016;58:52-58.
544 doi:10.1016/j.oraloncology.2016.05.008

545 7. Marabelle A, Le DT, Ascierto PA, et al. Efficacy of Pembrolizumab in Patients With Noncolorectal High Microsatellite
546 Instability/Mismatch Repair–Deficient Cancer: Results From the Phase II KEYNOTE-158 Study. *J Clin Oncol*.
547 Published online January 1, 2020. doi:10.1200/JCO.19.02105

548 8. Ino Y, Yamazaki-Itoh R, Shimada K, et al. Immune cell infiltration as an indicator of the immune microenvironment of
549 pancreatic cancer. *Br J Cancer*. 2013;108(4):914-923. doi:10.1038/bjc.2013.32

550 9. Gu H, Deng W, Zheng Z, Wu K, Sun F. CCL2 produced by pancreatic ductal adenocarcinoma is essential for the
551 accumulation and activation of monocytic myeloid-derived suppressor cells. *Immun Inflamm Dis*. 2021;9(4):1686-
552 1695. doi:10.1002/iid3.523

553 10. Blise KE, Sivagnanam S, Betts CB, et al. Machine Learning Links T-cell Function and Spatial Localization to
554 Neoadjuvant Immunotherapy and Clinical Outcome in Pancreatic Cancer. *Cancer Immunol Res*. 2024;12(5):544-558.
555 doi:10.1158/2326-6066.CIR-23-0873

556 11. Krenz B, Gebhardt-Wolf A, Ade CP, et al. MYC- and MIZ1-Dependent Vesicular Transport of Double-Strand
557 RNA Controls Immune Evasion in Pancreatic Ductal Adenocarcinoma. *Cancer Res*. 2021;81(16):4242-4256.
558 doi:10.1158/0008-5472.CAN-21-1677

559 12. Blanco FF, Jimbo M, Wulfkuhle J, et al. The mRNA-binding protein HuR promotes hypoxia-induced
560 chemoresistance through posttranscriptional regulation of the proto-oncogene PIM1 in pancreatic cancer cells.
561 *Oncogene*. 2016;35(19):2529-2541. doi:10.1038/onc.2015.325

562 13. Zarei M, Lal S, Parker SJ, et al. Posttranscriptional Upregulation of IDH1 by HuR Establishes a Powerful
563 Survival Phenotype in Pancreatic Cancer Cells. *Cancer Res*. 2017;77(16):4460-4471. doi:10.1158/0008-5472.CAN-17-
564 0015

565 14. Chang CH, Qiu J, O'Sullivan D, et al. Metabolic Competition in the Tumor Microenvironment Is a Driver of
566 Cancer Progression. *Cell*. 2015;162(6):1229-1241. doi:10.1016/j.cell.2015.08.016

567 15. Li W, Pan X, Chen L, et al. Cell metabolism-based optimization strategy of CAR-T cell function in cancer
568 therapy. *Front Immunol*. 2023;14. doi:10.3389/fimmu.2023.1186383

569 16. Lal S, Burkhart RA, Beeharry N, et al. HuR post-transcriptionally regulates WEE1: Implications for the DNA
570 damage response in pancreatic cancer cells. *Cancer Res*. 2014;74(4):1128-1140. doi:10.1158/0008-5472.CAN-13-1915

571 17. Brown SZ, McCarthy GA, Carroll JR, et al. The RNA-Binding Protein HuR Posttranscriptionally Regulates the
572 Protumorigenic Activator YAP1 in Pancreatic Ductal Adenocarcinoma. *Mol Cell Biol*. 2022;42(7):e00018-22.
573 doi:10.1128/mcb.00018-22

574 18. Kim HH, Yang X, Kuwano Y, Gorospe M. Modification at HuR(S242) Alters HuR Localization and Proliferative
575 Influence. *Cell Cycle Georget Tex*. 2008;7(21):3371-3377.

576 19. Anand S, Khan MA, Zubair H, et al. MYB sustains hypoxic survival of pancreatic cancer cells by facilitating
577 metabolic reprogramming. *EMBO Rep*. 2023;24(3):e55643. doi:10.15252/embr.202255643

578 20. Huang F, Bu L, Li M, et al. HuR/miR-124-3p/VDR complex bridges lipid metabolism and tumor development in
579 colorectal cancer. Published online March 1, 2023. doi:10.21203/rs.3.rs-2587383/v1

580 21. Osma-Garcia IC, Capitan-Sobrino D, Mouysset M, et al. The RNA-binding protein HuR is required for
581 maintenance of the germinal centre response. *Nat Commun*. 2021;12(1):6556. doi:10.1038/s41467-021-26908-2

582 22. Shao Z, Tu Z, Shi Y, et al. RNA-Binding Protein HuR Suppresses Inflammation and Promotes Extracellular
583 Matrix Homeostasis via NKRF in Intervertebral Disc Degeneration. *Front Cell Dev Biol*. 2020;8:611234.
584 doi:10.3389/fcell.2020.611234

585 23. Peng W, Furuuchi N, Aslanukova L, et al. Elevated HuR in Pancreas Promotes a Pancreatitis-Like Inflammatory
586 Microenvironment That Facilitates Tumor Development. *Mol Cell Biol*. 2018;38(3):e00427-17.
587 doi:10.1128/MCB.00427-17

588 24. McCarthy GA, Di Niro R, Finan JM, et al. Deletion of the mRNA stability factor ELAVL1 (HuR) in pancreatic
589 cancer cells disrupts the tumor microenvironment integrity. *NAR Cancer*. 2023;5(2):zcad016.
590 doi:10.1093/narcan/zcad016

591 25. Hingorani SR, Wang L, Multani AS, et al. Trp53R172H and KrasG12D cooperate to promote chromosomal
592 instability and widely metastatic pancreatic ductal adenocarcinoma in mice. *Cancer Cell*. 2005;7(5):469-483.
593 doi:10.1016/j.ccr.2005.04.023

594 26. Li M, Zhang X, Ang KS, et al. DISCO: a database of Deeply Integrated human Single-Cell Omics data. *Nucleic*
595 *Acids Res*. 2022;50(D1):D596-D602. doi:10.1093/nar/gkab1020

596 27. Nofech-Mozes I, Soave D, Awadalla P, Abelson S. Pan-cancer classification of single cells in the tumour
597 microenvironment. *Nat Commun*. 2023;14(1):1615. doi:10.1038/s41467-023-37353-8

598 28. Link JM, Eng JR, Pelz C, et al. Ongoing replication stress tolerance and clonal T cell responses distinguish liver
599 and lung recurrence and outcomes in pancreatic cancer. *Nat Cancer*. Published online January 9, 2025:1-22.
600 doi:10.1038/s43018-024-00881-3

601 29. Subramanian A, Tamayo P, Mootha VK, et al. Gene set enrichment analysis: a knowledge-based approach for
602 interpreting genome-wide expression profiles. *Proc Natl Acad Sci U S A*. 2005;102(43):15545-15550.
603 doi:10.1073/pnas.0506580102

604 30. Liberzon A, Birger C, Thorvaldsdóttir H, Ghandi M, Mesirov JP, Tamayo P. The Molecular Signatures Database
605 (MSigDB) hallmark gene set collection. *Cell Syst*. 2015;1(6):417-425. doi:10.1016/j.cels.2015.12.004

606 31. Zhang Y, Liu T, Meyer CA, et al. Model-based Analysis of ChIP-Seq (MACS). *Genome Biol*. 2008;9(9):R137.
607 doi:10.1186/gb-2008-9-9-r137

608 32. Lal S, Cheung EC, Zarei M, et al. CRISPR Knockout of the HuR Gene Causes a Xenograft Lethal Phenotype.
609 *Mol Cancer Res*. 2017;15(6):696-707. doi:10.1158/1541-7786.MCR-16-0361

610 33. Carstens JL, Correa de Sampaio P, Yang D, et al. Spatial computation of intratumoral T cells correlates with
611 survival of patients with pancreatic cancer. *Nat Commun*. 2017;8(1):15095. doi:10.1038/ncomms15095

612 34. Richards NG, Rittenhouse DW, Freydin B, et al. HuR Status is a Powerful Marker for Prognosis and Response to
613 Gemcitabine-Based Chemotherapy for Resected Pancreatic Ductal Adenocarcinoma Patients. *Ann Surg*.
614 2010;252(3):499. doi:10.1097/SLA.0b013e3181f1fd44

615 35. Collier C, Wucherer K, McWhorter M, et al. Intracellular K+ Limits T-cell Exhaustion and Preserves Antitumor
616 Function. *Cancer Immunol Res*. 2024;12(1):36-47. doi:10.1158/2326-6066.CIR-23-0319

617 36. Fridman WH, Pagès F, Sautès-Fridman C, Galon J. The immune contexture in human tumours: impact on clinical
618 outcome. *Nat Rev Cancer*. 2012;12(4):298-306. doi:10.1038/nrc3245

619 37. Rothamel K, Arcos S, Kim B, et al. ELAVL1 primarily couples mRNA stability with the 3′ UTRs of interferon-
620 stimulated genes. *Cell Rep*. 2021;35(8):109178. doi:10.1016/j.celrep.2021.109178

621 38. Antal CE, Oh TG, Aigner S, et al. A super-enhancer-regulated RNA-binding protein cascade drives pancreatic
622 cancer. *Nat Commun*. 2023;14(1):5195. doi:10.1038/s41467-023-40798-6

623 39. Hanahan D, Weinberg RA. Hallmarks of Cancer: The Next Generation. *Cell*. 2011;144(5):646-674.
624 doi:10.1016/j.cell.2011.02.013

625 40. Sullivan MR, Danai LV, Lewis CA, et al. Quantification of microenvironmental metabolites in murine cancers
626 reveals determinants of tumor nutrient availability. DeBerardinis R, van Lohuizen M, DeBerardinis R, Frezza C, eds.
627 *eLife*. 2019;8:e44235. doi:10.7554/eLife.44235

628 41. Kidani Y, Elsaesser H, Hock MB, et al. Sterol regulatory element–binding proteins are essential for the metabolic
629 programming of effector T cells and adaptive immunity. *Nat Immunol*. 2013;14(5):489-499. doi:10.1038/ni.2570

630 42. Leone RD, Powell JD. Metabolism of immune cells in cancer. *Nat Rev Cancer*. 2020;20(9):516-531.
631 doi:10.1038/s41568-020-0273-y

632 43. Yan Y, Huang L, Liu Y, et al. Metabolic profiles of regulatory T cells and their adaptations to the tumor
633 microenvironment: implications for antitumor immunity. *J Hematol OncolJ Hematol Oncol*. 2022;15:104.
634 doi:10.1186/s13045-022-01322-3

635 44. Morrison AH, Diamond MS, Hay CA, Byrne KT, Vonderheide RH. Sufficiency of CD40 activation and immune
636 checkpoint blockade for T cell priming and tumor immunity. *Proc Natl Acad Sci U S A*. 2020;117(14):8022-8031.
637 doi:10.1073/pnas.1918971117

638 45. Kenkel JA, Tseng WW, Davidson MG, et al. An Immunosuppressive Dendritic Cell Subset Accumulates at
639 Secondary Sites and Promotes Metastasis in Pancreatic Cancer. *Cancer Res*. 2017;77(15):4158-4170.
640 doi:10.1158/0008-5472.CAN-16-2212

641 46. Finan JM, Sutton TL, Dixon DA, Brody JR. Targeting the RNA-Binding Protein HuR in Cancer. *Cancer Res*.
642 2023;83(21):3507-3516. doi:10.1158/0008-5472.CAN-23-0972

643

Figure 1

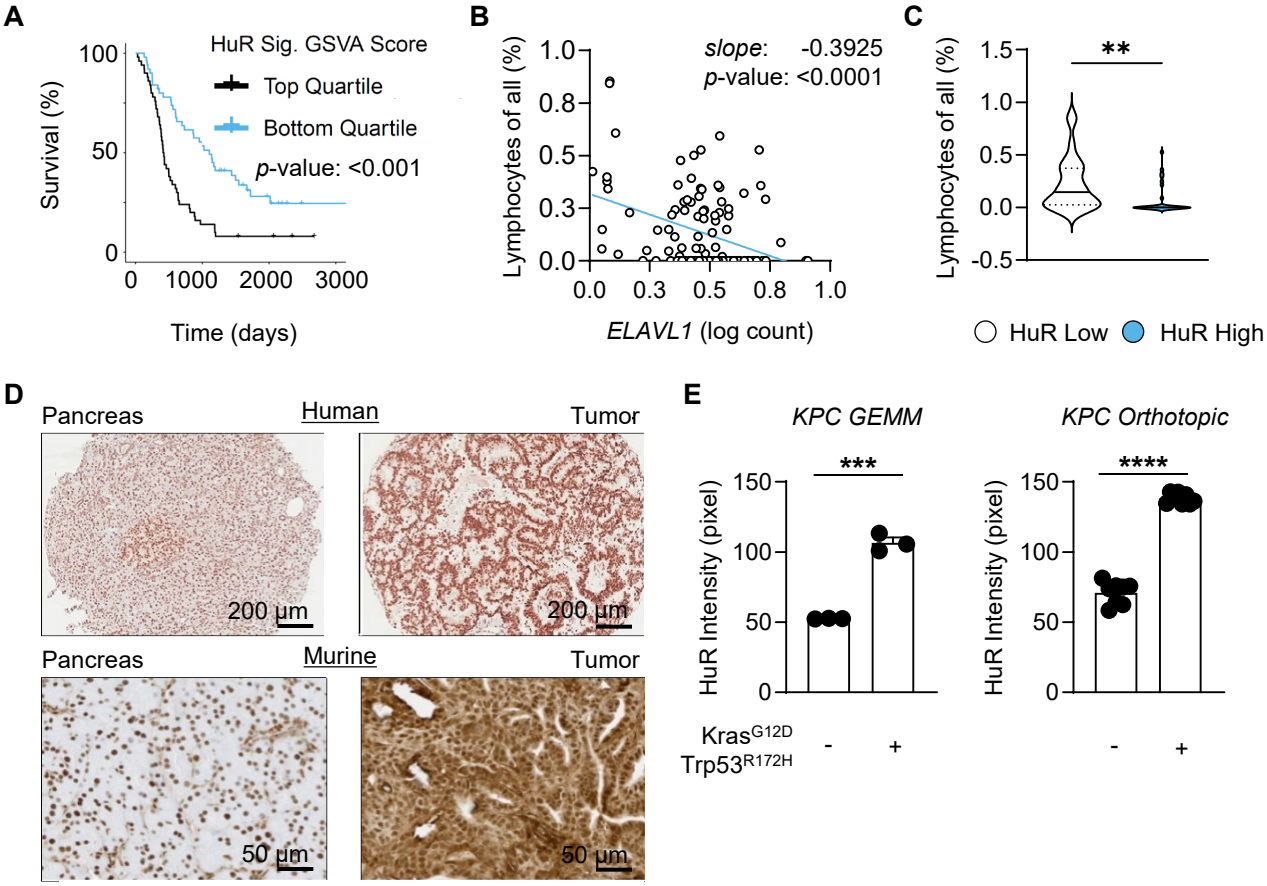
A
HuR Sig. GSVA Score
Top Quartile
Bottom Quartile
p-value: <0.001
Survival (%)
100
50
0
0
1000
2000
3000
Time (days)
B
slope: -0.3925
p-value: <0.0001
Lymphocytes of all (%)
1.0
0.8
0.5
0.3
0.0
0.0
0.3
0.5
0.8
1.0
ELAVL1 (log count)
C
**
Lymphocytes of all (%)
1.5
1.0
0.5
0.0
-0.5
HuR Low
HuR High
D
Pancreas
Human
Tumor
200 µm
200 µm
Pancreas
Murine
Tumor
50 µm
50 µm
E
KPC GEMM
KPC Orthotopic
***
****
HuR Intensity (pixel)
150
100
50
0
KrasG12D
Trp53R172H
-
+
-
+

Figure 2

A

Clone	ICE	KO-Score	R^2	Indels
KO6	80	74	0.8	{'1': 7.0, '-1': 67.0, '-3': 6.0}
KO8	97	97	0.97	{'-1': 97.0}
KO9	93	93	0.93	{'-1': 83.0, '-2': 10.0}

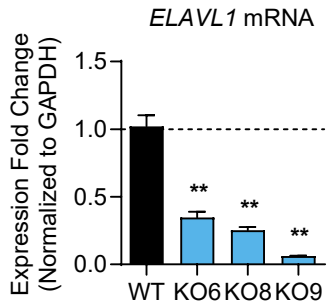

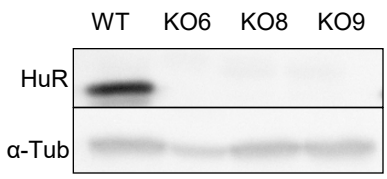

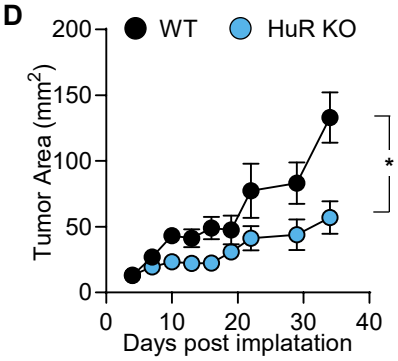

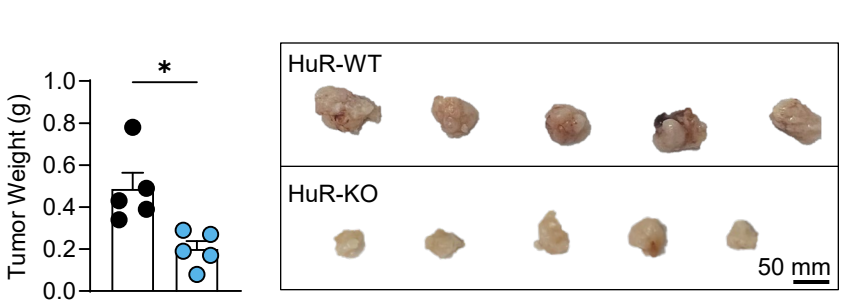

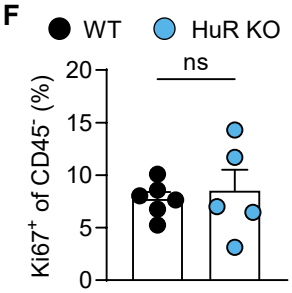

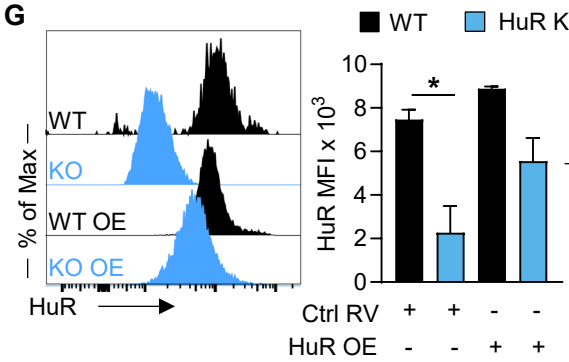

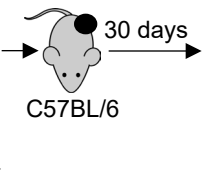

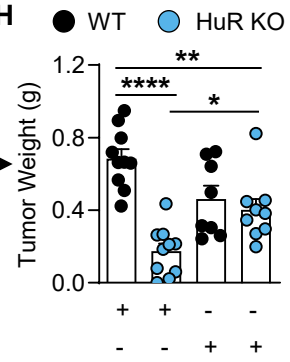

Figure 3

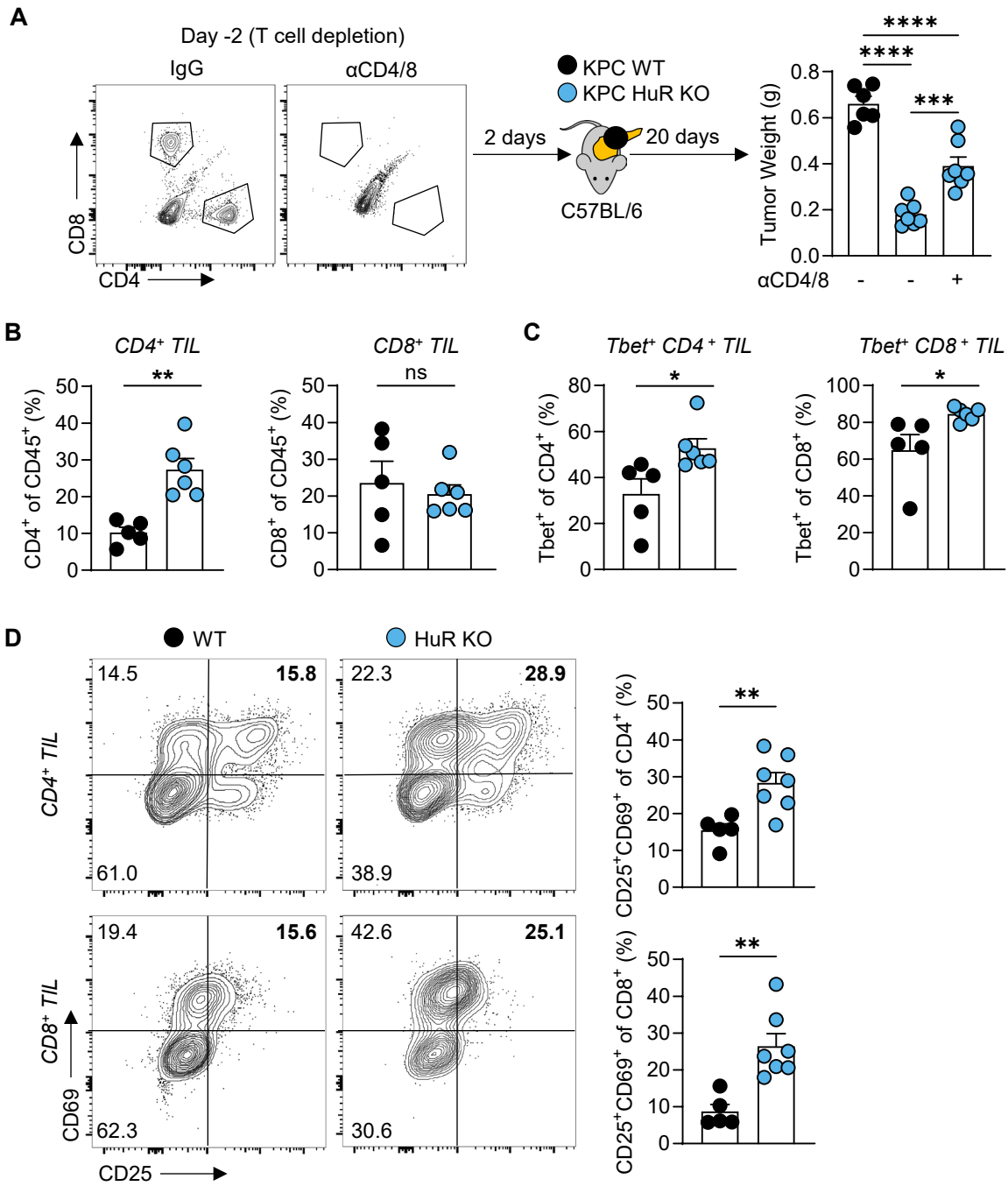
A
Day -2 (T cell depletion)
IgG
αCD4/8
CD8
CD4
2 days
KPC WT
KPC HuR KO
20 days
C57BL/6
Tumor Weight (g)
αCD4/8
B
CD4+ TIL
CD8+ TIL
CD4+ of CD45+ (%)
CD8+ of CD45+ (%)
ns
C
Tbet+ CD4+ TIL
Tbet+ CD8+ TIL
Tbet+ of CD4+ (%)
Tbet+ of CD8+ (%)
D
WT
HuR KO
CD4+ TIL
CD8+ TIL
CD69
CD25
CD25+CD69+ of CD4+ (%)
CD25+CD69+ of CD8+ (%)

Figure 4

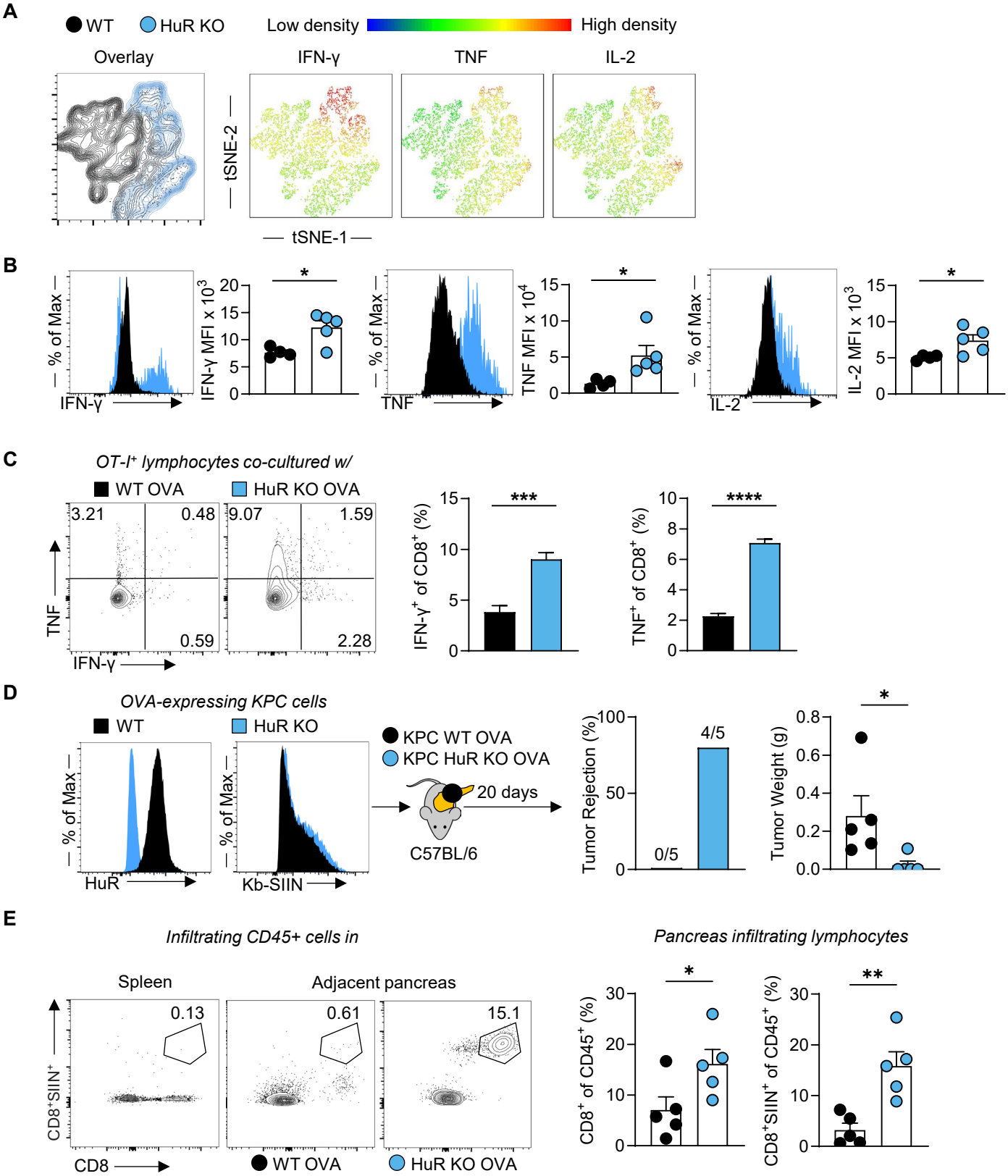
A
WT
HuR KO
Low density
High density
Overlay
IFN-γ
TNF
IL-2
tSNE-2
tSNE-1
B
% of Max
IFN-γ
IFN-γ MFI x 10^3
TNF
TNF MFI x 10^4
IL-2
IL-2 MFI x 10^3
C
OT-I+ lymphocytes co-cultured w/
WT OVA
HuR KO OVA
3.21
0.48
0.59
9.07
1.59
2.28
TNF
IFN-γ
IFN-γ+ of CD8+ (%)
TNF+ of CD8+ (%)
D
OVA-expressing KPC cells
WT
HuR KO
HuR
Kb-SIIN
KPC WT OVA
KPC HuR KO OVA
20 days
C57BL/6
Tumor Rejection (%)
0/5
4/5
Tumor Weight (g)
E
Infiltrating CD45+ cells in
Spleen
Adjacent pancreas
0.13
0.61
15.1
CD8+SIIN+
CD8
WT OVA
HuR KO OVA
Pancreas infiltrating lymphocytes
CD8+ of CD45+ (%)
CD8+SIIN+ of CD45+ (%)

Figure 5

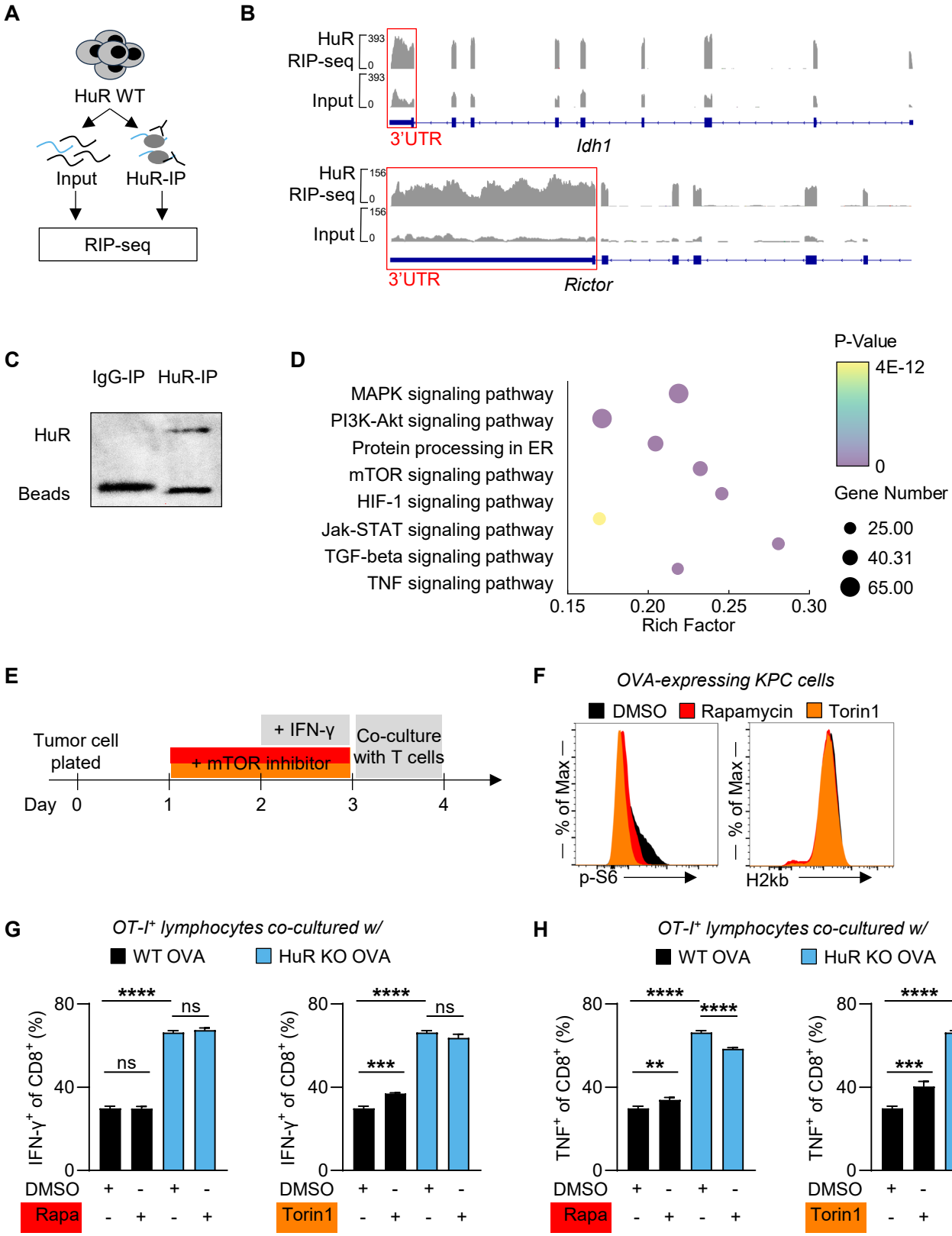
A
HuR WT
Input
HuR-IP
RIP-seq
B
HuR RIP-seq
Input
3'UTR
Idh1
Rictor
C
IgG-IP
HuR-IP
HuR
Beads
D
MAPK signaling pathway
PI3K-Akt signaling pathway
Protein processing in ER
mTOR signaling pathway
HIF-1 signaling pathway
Jak-STAT signaling pathway
TGF-beta signaling pathway
TNF signaling pathway
Rich Factor
P-Value
4E-12
0
Gene Number
25.00
40.31
65.00
E
Tumor cell plated
+ IFN-γ
+ mTOR inhibitor
Co-culture with T cells
Day
F
OVA-expressing KPC cells
DMSO
Rapamycin
Torin1
% of Max
p-S6
H2kb
G
OT-I+ lymphocytes co-cultured w/
WT OVA
HuR KO OVA
IFN-γ+ of CD8+ (%)
DMSO
Rapa
Torin1
H
TNF+ of CD8+ (%)

Figure 6

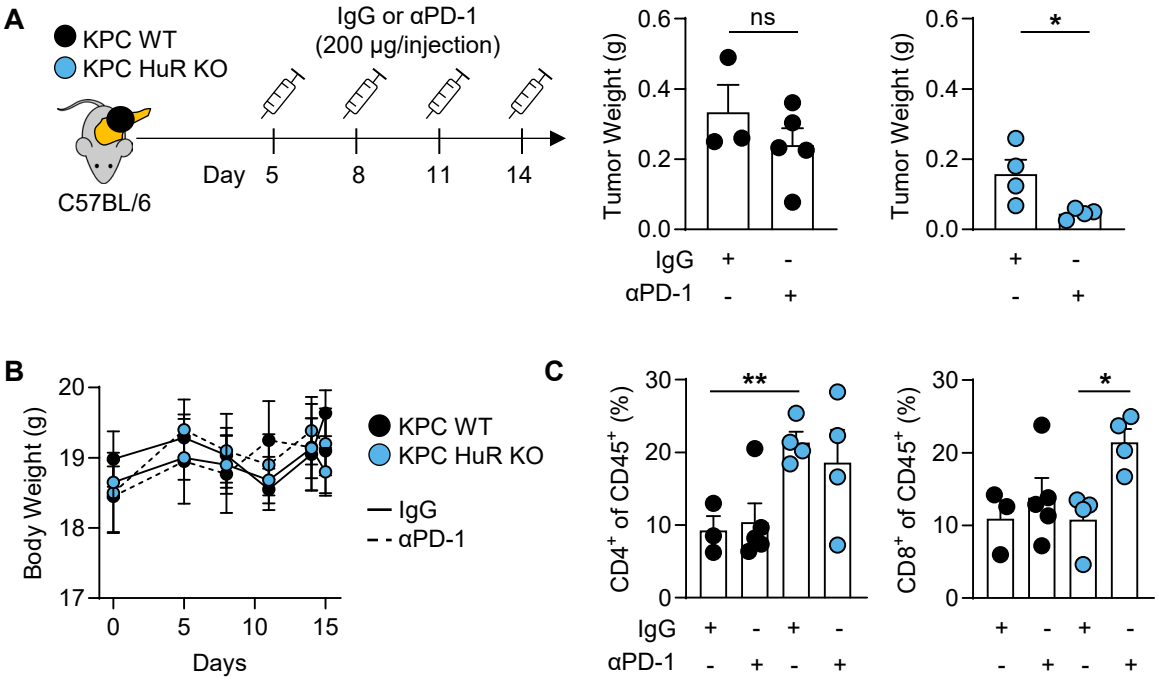
A
KPC WT
KPC HuR KO
IgG or αPD-1
(200 μg/injection)
Day 5 8 11 14
C57BL/6
Tumor Weight (g)
ns
*
IgG + -
αPD-1 - +
B
Body Weight (g)
Days
KPC WT
KPC HuR KO
IgG
αPD-1
C
CD4+ of CD45+ (%)
CD8+ of CD45+ (%)
**
*
IgG + - + -
αPD-1 - + - +

Supplement Figure 1

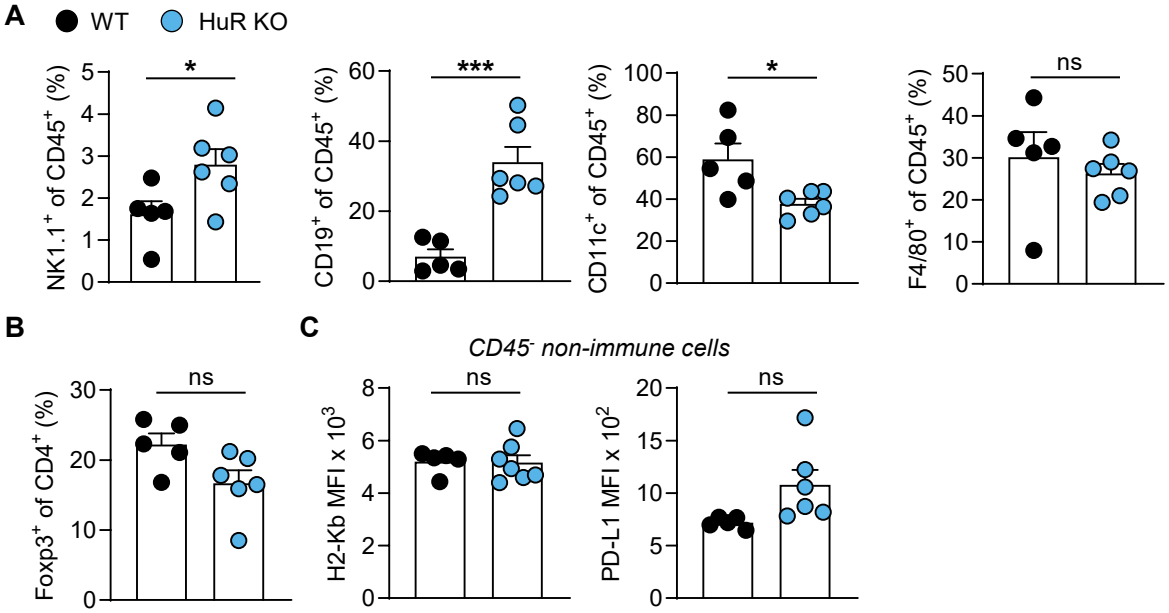

Supplement Figure 2

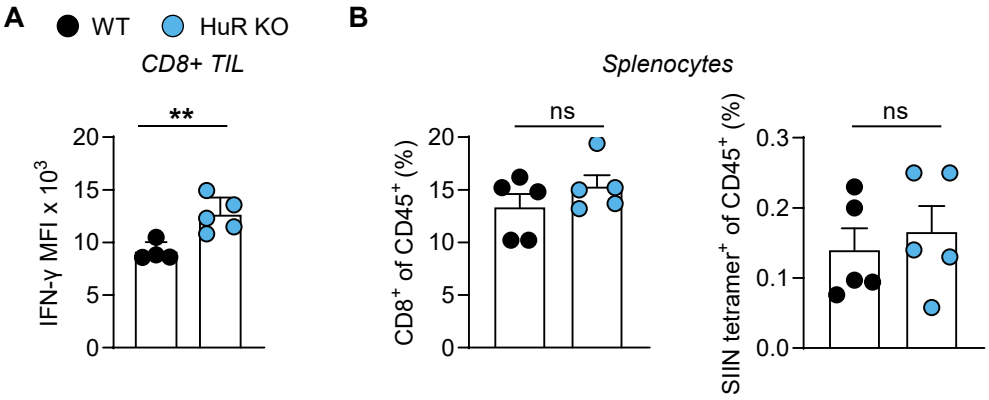

Supplement Figure 3

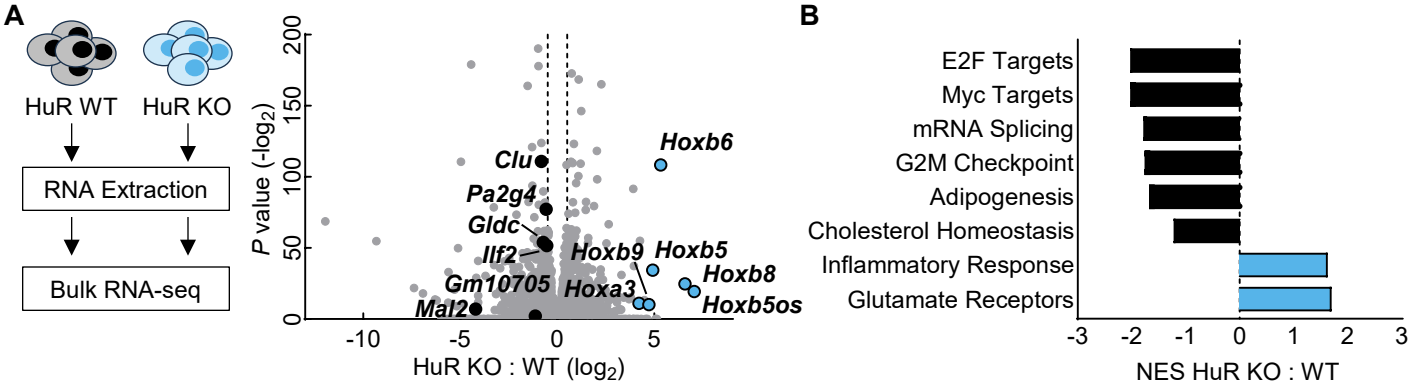

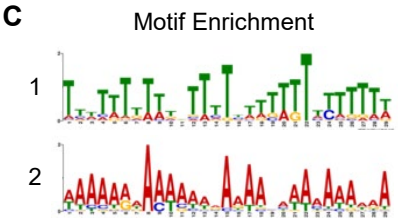

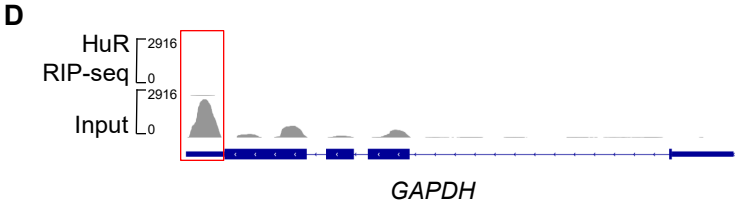

Supplemental Table 1. Flow cytometry antibodies.

Marker	**Flour**
CD11c	BV650
CD19	BV711
CD25	BV421
CD4	PCP-Cy5.5
CD4	BUV805
CD45	AF700
CD62L	BUR395
CD69	APC-Cy7
CD8	FITC
CD8	APC-Cy7
CD90.2	BV786
F4/80	BV421
FasL	PE
Foxp3	PE
GranzB	PE
IFNg	APC
IL-2	FITC
Ki67	BUV805
LiveDead	Aqua
MHC-I	FITC
MHC-II	APC-Cy7
NK1.1	PE-Cy7
PD-1	APC
PD-L1	APC
TBET	PE-Cy7
Tim3	BV650
TNF	BV421